Rational design of polyaromatic ionomers for alkaline membrane fuel cells with > 1 W cm^{-2} power density

Journal:	*Energy & Environmental Science*
Manuscript ID	EE-ART-07-2018-002192.R2
Article Type:	Paper
Date Submitted by the Author:	12-Sep-2018

Complete List of Authors:	Maurya, Sandip; Los Alamos National Laboratory, MPA-11: Materials Synthesis and Integrated Devices Noh, Sangtaik; Rensselaer Polytechnic Institute, Matanovic, Ivana; University of New Mexico, Park, Eun Joo; Los Alamos National Laboratory, Narvaez Villarrubia, Claudia; Los Alamos National Laboratory, a. Physical Chemistry and Applied Spectroscopy (C-PCS), Chemistry Division; Los Alamos National Laboratory, mpa-11, Material Synthesis and Integrated Devices Martinez, Ulises; Los Alamos National Laboratory, Materials Physics and Applications; University of New Mexico, Center for Emerging Energy Technologies, Department of Chemical and Nuclear Engineering Han, Junyoung; Rensselaer Polytechnic Institute Bae, Chulsung; Rensselaer Polytechnic Institute, Chemistry & Chemical Biology Kim, Yu Seung; Los Alamos National Laboratory,

Broader context for Rational Design of Polyaromatic Ionomers for Alkaline Membrane Fuel Cells with 1 W cm^{-2} Power Density by Maurya et al.

Fuel cells are electrochemical energy conversion devices that have the potential to provide clean, sustainable energy for stationary and transportation applications. Proton exchange membrane fuel cells (PEMFCs) that use a water-based, acidic polymer membrane with platinum-based electrodes are currently the leading technology for automotive applications. Over the last decade, alkaline membrane fuel cells (AMFCs) have drawn a lot of interest due to the use of inexpensive platinum group metal-free catalysts for the oxygen reduction reaction. However, reported performance of most AMFCs was low, and the cause of the poor performance was unclear. This study suggests that the phenyl group adsorption of the ionomeric binder on hydrogen oxidation catalyst may be the primary cause for the low AMFC performance. By preparing new ionomer with less phenyl group adsorbing characteristics, we demonstrate an AMFC with a performance comparable to that of PEMFCs. The lessons learned from this work can also be applied to other electrochemical energy devices in which polymer electrolytes interact with electrocatalysts.

Journal Name

ARTICLE

Rational design of polyaromatic ionomers for alkaline membrane fuel cells with > 1 W cm^{-2} power density

Received 00th January 20xx,
Accepted 00th January 20xx

DOI: 10.1039/x0xx00000x

www.rsc.org/

Sandip Maurya,†[a] Sangtaik Noh,†[b] Ivana Matanovic,†[cd] Eun Joo Park,[a] Claudia Narvaez Villarrubia,[a] Ulises Martinez,[a] Junyoung Han,[b] Chulsung Bae,*[b] and Yu Seung Kim*[a]

Alkaline membrane fuel cells (AMFCs) show great potential as the alternative energy conversion devices to acidic proton exchange membrane fuel cells (PEMFCs). Over the last decade, there has been significant progress in the development of alkaline-stable polyaromatic materials for the membrane separators and ionomeric binders for AMFCs. However, the AMFC performance using polyaromatic ionomers is generally poor, *ca.* peak power density of < 400 mW cm^{-2}. Here, we report a rational design for polyaromatic ionomers which can minimize undesirable phenyl group interaction with hydrogen oxidation catalysts. The AMFC using a newly designed aryl ether-free poly(fluorene) ionomer exhibits the peak power density of 1.46 W cm^{-2}, which is approaching that of Nafion-based PEMFCs. This study further discusses the remaining challenges of high-performing AMFCs.

Introduction

Alkaline membrane fuel cells (AMFCs) have emerged as an attractive technology for energy conversion devices, with the potential advantages of utilizing low-cost platinum-group metal-free (PGM-free) catalysts and less expensive metal hardware under high pH conditions.[1] The AMFC performance and durability are affected by many fuel cell components and operating parameters. Polymer electrolytes used as hydroxide-conducting membrane separator (anion exchange membrane) and electrode binder (ionomer) play a critical role in the performance of AMFCs. [2-4]

Quaternized polyaromatics are one of the most studied alkaline electrolytes because of their availability, processability, good hydroxide conductivity, and anticipated oxidative and hydrolytic stability under high pH conditions.[5] Since Zschocke and Quellmalz demonstrated the stability of a non-quaternized poly(aryl ether sulfone) under high pH conditions,[6] researchers have prepared many quaternized polyaromatics for AMFC applications over the past two decades.[7-21] The most popular ones are quaternized poly(aryl ether sulfone)s (PAESs), prepared *via* the polycondensation reaction between aromatic dihalides and dihydroxy monomers followed by chloromethylation and subsequent quaternary amination.

A significant molecular design change of quaternized polyaromatics occurred in the early 2010s as our and other research groups reported that the polymer backbone of quaternized PAESs readily degrades under high pH conditions *via* aryl ether cleavage reaction.[19, 22-25] These studies led the structural change of quaternized polyaromatics to quaternized poly(phenylene oxide)s (PPOs) which have no significant electron-withdrawing groups in the polymer backbone[26-31] or aryl ether-free quaternized poly(phenylene)s (PPs)[32-34]. The molecular design transition to quaternized PPOs and PPs occurred with additional changes in a cationic group tethered side chain. Pan et al. proposed a multi-cation functionalized side chain that reduces the grafting degree of functional groups to improve the backbone stability of quaternized PPOs.[35] This approach has become prominent as others showed that the multi-cation side chain also enhanced the hydroxide conductivity.[36-39] An alternative approach to improve the backbone stability of quaternized PPOs is to introduce long alkyl chain spacers between the polymer backbone and cationic functional group.[40-49] This approach has also been implemented in the preparation of quaternized PPs because long alkyl spacers enhance the stability of the cationic functional group as well as the polymer backbone.[50] The quaternized PPs with pendant quaternary ammonium alkyl groups exhibited excellent alkaline stability.[51]

While current quaternized PPO and PP ionomers have achieved relatively good alkaline stability, the AMFCs of membrane electrode assemblies (MEAs) employing the polyaromatic ionomers have exhibited poor performance. Figure 1 compares the peak power density of AMFCs

[a] *MPA-11: Materials Synthesis & Integrated Devices, Los Alamos National Laboratory, Los Alamos, New Mexico 87545, USA*
[b] *Department of Chemistry and Chemical Biology, Rensselaer Polytechnic Institute, Troy, New York 12180, USA*
[c] *Department of Chemical and Biological Engineering, Center for Micro-Engineered Materials (CMEM), The University of New Mexico, Albuquerque, New Mexico 87231, USA*
[d] *Theoretical Division, Los Alamos National Laboratory, Los Alamos 87545, USA*
† Equal Contributors
Electronic Supplementary Information (ESI) available: [Experimental Procedure, DFT modelling, Materials and Method and Fuel Cell Data]. See DOI: 10.1039/x0xx00000x

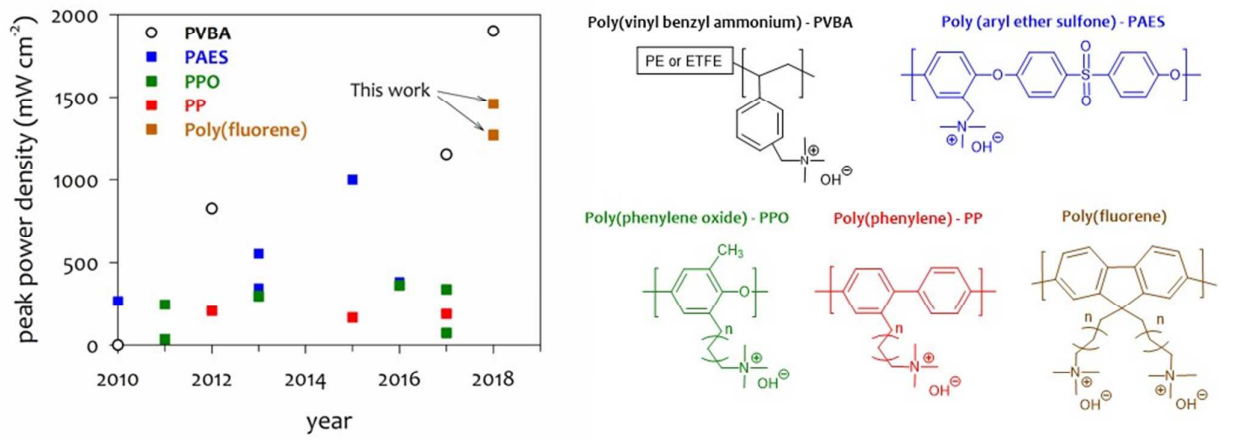

Figure 1. AMFC performance under H_2/O_2 conditions using polyaromatic ionomers; the performance of AMFCs using grafted PVBA ionomers are shown for comparison. Data taken from refs. [57-60] for PVBA, refs. [19-21, 52] for PAES, refs. [29, 45, 46, 53-55] for PPO, and refs. [19, 32, 34, 56] for PP.

employing different types of ionomer (note that the data shown in Fig. 1 represent the best AMFC performance reported under different conditions). While the peak power density of AMFC using a less-alkaline stable PAES ionomer has been demonstrated to reach 1 W cm^{-2},[52] the peak power densities of AMFCs employing PPOs with alkyl or multi-cation side chain are < 400 mW cm^{-2}.[29, 45, 46, 53-55] The AMFC performance of MEAs using aryl ether-free PP ionomers is even lower, *ca*. peak power density < 300 mW cm^{-2}.[19, 32, 34, 56] In contrast, the MEAs employing grafted poly(vinyl benzyl ammonium) (PVBA) ionomers have achieved up to 1,900 mW cm^{-2} peak power density.[57-60] The significantly lower performance of MEAs using the alkaline stable polyaromatic ionomers suggests that further structural changes for the polyaromatic ionomers may be necessary.

Recently, we have proposed that phenyl group adsorption on electrocatalysts is a major performance-limiting factor for polyaromatic ionomers as the adsorbed phenyl group inhibits the hydrogen oxidation reaction (HOR).[61] The rotating disk electrode experiments and Density Functional Theory (DFT) calculation study indicated that when phenyl groups of benzyl ammonium have the orientation parallel to the catalyst surface, the alkaline HOR significantly reduced. We proposed that the phenyl groups were less adsorbed on the surface of Pt-Ru alloy catalysts. In a subsequent paper,[62] we demonstrated that the Pt-Ru catalysed AMFCs using an aryl ether-free Diels Alder PP ionomer improved the AMFC peak power density from 220 to 460 mW cm^{-2}. Further performance improvement up to 650 mW cm^{-2} peak power density achieved with a less-phenyl group containing Diels Alder PP ionomer. These results confirmed that the adsorption of phenyl groups is the major performance-limiting factor. However, the improved performance of the AMFCs after implementing those mitigation strategies is still far below the AMFC performance of MEAs employing the state-of-the-art PVBA ionomers. This means that a new material design approach is needed for polyaromatic ionomers to maximize desirable properties of quaternized polyaromatics such as good processability.

Our new design concept comes from the hypothesis that non- rotatable phenyl-phenyl rings in the polyaromatic backbone may minimize phenyl group interaction with electrocatalysts. From this hypothesis, we have paid attention to poly(fluorene)s which have central fused five-membered ring between two phenyl-groups providing non-rotating polymer backbone characteristics. Several quaternized poly(fluorene)s have been synthesized for AMFC applications; however, most of the quaternized poly(fluorene)s have been incorporated with alkaline-unstable PAESs or not been tested in AMFCs.[63-67]

In this paper, we first compare the adsorption energies of two model compounds, i.e., biphenyl having rotatable phenyl groups and dimethyl fluorene having non-rotatable phenyl groups on the Pt and Pt-Ru alloy catalyst to prove our hypothesis regarding phenyl group adsorption. Then, we describe the synthesis of two types of ionomeric binders, i.e., alkyl ammonium tethered poly(fluorene)s (FLNs) and poly(biphenylene) (BPN) *via* acid catalysed polycondensation reaction. Direct evidence of phenyl adsorption is provided by infrared reflection absorption spectroscopy (IRRAS). We examine the impact of the phenyl group adsorption on HOR voltammograms by the thin ionomer-coated microelectrode experiments. Finally, we demonstrate the AMFC performance of two MEAs employing the structurally different ionomers. For a fair comparison, we demonstrate all AMFC performance with aryl ether-free poly(terphenylene) (TPN) membranes[32] having the same thickness (30 μm). Figure 2 shows the

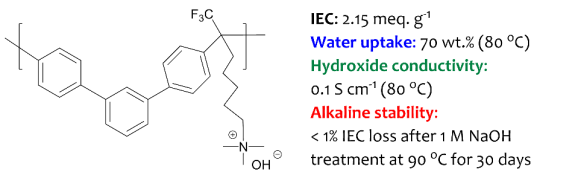

Figure 2. The chemical structure and electrochemical property of TPN.

chemical structure and electrochemical properties of TPN.

Results and discussion

Density functional theory calculation on phenyl group adsorption

The adsorption energy of two model compounds, i.e., biphenyl and 9,9-dimethyl fluorene on the Pt and Pt-Ru surface was calculated by DFT using the vdW-DF functional proposed by Dion et al.[68-70] This functional was previously tested and was shown as an optimal approach to correctly describe the interactions between the surface and the aromatic molecules by accounting for the dispersion interactions.[71]

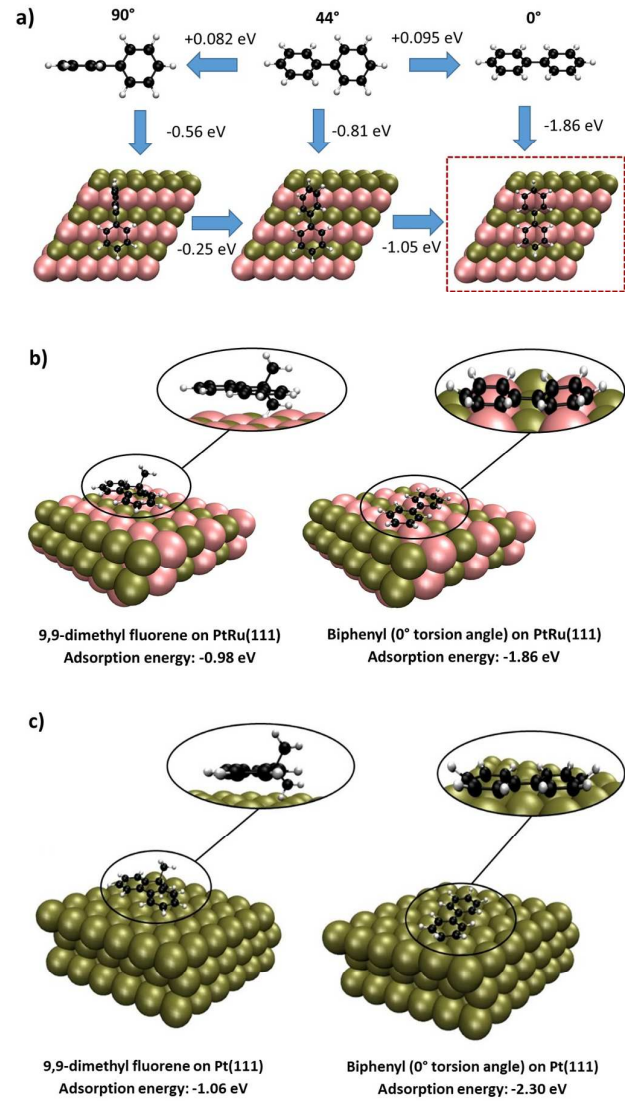

Figure. 3. (a) Relative stabilities of biphenyl in the gas phase and adsorbed on PtRu(111) surface as calculated using DFT. (b) and (c) Optimized geometries and adsorption energy (in eV) of 9,9-dimethyl fluorene and biphenyl adsorbed on PtRu(111) and Pt(111). Atoms belonging to one unit cell are shown. Pink = Ru, tan = Pt, black =C, white = H.

For biphenyl, three conformations with the torsion angles of 0°, 44°, and 90° between the phenyl rings were considered (Fig. 3a). In the gas phase, 44° conformation is found to be the most stable, which is in good agreement with the experiment and previous calculations.[72, 73] However, in the interaction with the Pt-Ru surface the conformation in which both phenyl rings are adsorbed parallel to the surface (0° conformation) becomes the most stable conformation on biphenyl. Namely, this conformation has the highest adsorption energy on Pt-Ru surface (Fig. 3a) and is -1.05 eV more stable than that of biphenyl with 44° torsion angle. Adsorption of biphenyl with both rings parallel to the surface (or parallel adsorption) allows for the highest overlap between the π-system of biphenyl and the *d*-band of the metal. The strong hybridization of the *p*-orbitals and bending of the benzene C-H bonds away from the surface in DFT optimized geometries has been shown before for extended metal surfaces where bonding with benzene is strong, such as Pt, Ni, and Rh.[74-76]

The analysis of the DFT optimized geometries (Fig. S1) further reveals that the average orthogonal distance between the carbon atoms of the biphenyl and the top layer of the metal surface is 2.30 Å, very similar to the distance of 2.05 Å, found in the case of benzene adsorption on Pt(111) and Pt3M alloys.[77] For 9,9-dimethyl fluorene, the methyl groups hinder closer positioning of the π-system of the dimethyl fluorene relative to the metal surface and prevent stronger interaction of this fragment with the catalytic surface. The orthogonal distance between the carbon atoms of the fluorene and the top catalyst layer is 3.87 Å, much larger than that of biphenyl. Consequently, the biphenyl adsorbs more strongly on the Pt-Ru catalyst surface than the dimethyl fluorene (Fig. 3b). Namely, the adsorption energies of biphenyl and dimethyl fluorene are calculated as -1.86 eV and -0.98 eV, respectively.

The adsorption energy of the dimethyl fluorene and biphenyl on Pt(111) was also calculated by DFT using vdW-DF functional (Fig. 3c). The adsorption energy of 9,9-dimethyl fluorene is similar with that on Pt-Ru surface (-1.06 eV), which indicates the adsorption of the phenyl group in the dimethyl fluorene molecule on both Pt and Pt-Ru catalysts is minimal, and thus poly(fluorene)-based ionomers can effectively prevent the adverse phenyl adsorption on both Pt and Pt-Ru catalysts to improve AMFC performance. In contrast, the adsorption energy of biphenyl on Pt surface is much higher (-2.30 eV), suggesting that the impact of replacing Pt catalyst with Pt-Ru catalyst is more significant with poly(biphenyl)-based ionomers.

Synthesis and characterization of FLN and BPN ionomers

Quaternized poly(fluorene)s (FLNs) were synthesized *via* one-pot, acid-catalysed Friedel-Crafts polycondensations of 1,1,1-trifluoroacetone and fluorene monomers and subsequent amination with trimethylamine (Fig. 4a). The ion exchange capacity (IEC) of FLNs was controlled by the feed ratio of 9,9-dimethylfuorene and 9,9-bis(6-bromohexyl)fluorene. The chemical structures of the pre-aminated polymer precursor and FLN were confirmed by ^{1}H NMR spectroscopies (Fig. S2).

By comparing the integral ratio of the peak at 3.22 ppm (from the -CH_2Br peak of 9,9-bis(6-bromohexyl)fluorene) and the peak at 2.01 ppm (from the –CF_3CCH_3– of the backbone) of the precursor polymer, it was confirmed that the incorporation of monomer matches well with feed ratio. After conversion to quaternary ammonium group in the ionomer, the appearance of a new proton peak at 3.00 ppm (from the –$N^+(CH_3)_3$) indicates full conversion of the reaction (Fig. S3). Quaternized

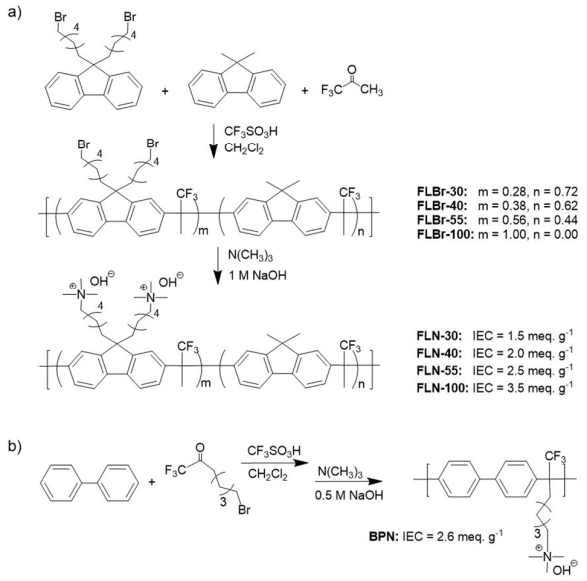

Figure. 4. Synthetic scheme of (a) FLNs and (b) BPN ionomers.

poly(biphenylene) ionomer (BPN) (Fig. 4b) was also synthesized using the synthetic procedure from our previous report.[32] The chemical structures of the polymer precursor before amination and BPN were confirmed by ^{1}H NMR spectroscopies (Fig. S4).

Table 1 summarises the electrochemical properties of FLNs and BPN. The IECs of the ionomers measured by the ^{1}H NMR ranged from 1.6 to 3.5 meq. g^{-1}, which are in good agreement from theoretical calculations. The water uptake (WU) of FLNs increased from 30 to 180 wt% as the IEC of FLNs increased from 1.6 to 2.5 meq. g^{-1}. However, we could not accurately measure the water uptake of FLN-100 because of the excessive swelling of the polymer; the water uptake estimated from the polymer hydrogel is at least 2,000 wt%. The water uptake of BPN was 145 wt%, ~20% lower than that of FLN-55 (180 wt%), probably because of the higher free volume of FLN induced from the bulky structure. The hydroxide conductivity (σ) of FLNs measured at 30 °C increased from 36 to 110 mS cm^{-1} as the IEC increased from 1.6 to 2.5 meq. g^{-1}. However, the conductivity difference between FLNs is much smaller at 80 °C (105-127 mS cm^{-1}) because the FLNs with higher IEC have lower activation energy (E_a) due to a lower conduction barrier with the larger and more connected hydrophilic phase. The hydroxide conductivity of BPN is comparable to that of FLN-55 at 80 °C. The results of Table 1 indicated that BPN and FLN-55 have similar IEC and hydroxide conductivity, thus the impact of phenyl-phenyl rotation of the polymer backbones on phenyl group adsorption may stand out in the AMFC performance evaluation.

Table 1. Electrochemical properties of ionomers used for this study.

Iono-mer	IEC (meq. g^{-1})		WU[a] (wt%)	Swelling (%)	σ (mS cm^{-1})		E_a (kJ mol^{-1})
	Theo.	NMR			30 °C	80 °C	
FLN-30	1.5	1.6	30 ± 4	7	36 ± 5	105 ± 5	19.0
FLN-40	2.0	2.0	75 ± 7	13	55 ± 5	119 ± 5	13.7
FLN-55	2.5	2.5	180 ± 13	60	110 ± 5	120 ± 7	1.5
FLN-100	3.5	3.5	> 2000[b]	NA[c]	NA	NA	NA
BPN[d]	2.6	2.6	145	40	62	127	12.7

[a] measured in OH^- form at room temperature.
[b] gel formation.
[c] NA: not available
[d] taken from Ref. 32.

The chemical stability of the FLN and BPN ionomers under high pH conditions was evaluated by immersing the solvent-cast membranes in 1 M NaOH solution at 80 °C. The changes in IEC, hydroxide conductivity and chemical structure during the NaOH treatment was evaluated. Similar to the case of BPN,[32] the IECs and hydroxide conductivity for the FLN ionomers measured by titration after the 500 h NaOH treatment were identical to the initial value (Table S1). The alkaline-stability of FLNs and BPN was further confirmed by ^{1}H NMR spectra, which were taken for the FLN and BPN ionomers in OH^- form during the NaOH treatment (Figs. S5 and S6). No change in the chemical shift was observed after 30 days in 1 M NaOH at 80 °C. This result confirms that both the aryl ether-free FLN and BPN ionomers have excellent stability under high pH conditions and are suitable for practical use in AMFCs.

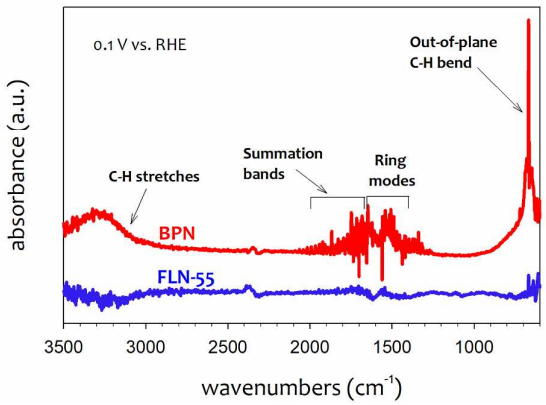

Figure 5. IRRAS spectra of the BPN and FLN-55 coated polycrystalline Pt electrode at 0.1 V vs. RHE. The spectra was measured after preconditioning of the electrode at 1.4 V vs. RHE for 30 sec.

IRRAS study on phenyl group adsorption

IRRAS experiments were performed to investigate the phenyl adsorption on the surface of a Pt disc electrode. For these experiments, a thin film of ionomer (BPN or FLN-55) was drop-casted on top of the Pt disc electrode. Prior to collecting the IRRAS spectra, a background spectrum was collected while holding the potential of the electrode at 1.4 V vs. RHE.[78] Adsorption studies were carried out by recording a series of IR spectra at 0.1 V vs. RHE (Fig. 5). The characteristic peaks of adsorbed species were obtained after subtracting the reference background for water of the liquid electrolyte (in- and out-of-phase O-H stretch at 3600–3000 cm^{-1}, and H-O-H bend near 1600 cm^{-1}). The IRRAS spectrum of BPN-coated Pt electrode shows phenyl characteristic peaks at 3100–3000 cm^{-1} (C-H stretches), 2000–1670 cm^{-1} (summation bands), 1660–1400 cm^{-1} (ring mode) and 670 cm^{-1} (out-of-plane C-H bend), although the C-H stretch peak at 3100–3000 cm^{-1} and the ring modes at 1660–1400 cm^{-1} are masked by the vibrational frequencies of water occurring in the same region. The characteristic peak of in-plane C-H bending mode at ~1100 cm^{-1} is missing, suggesting that the atoms in the adsorbed phenyl groups are not located in the same plane. The absence of the in-plane C-H bending mode is also consistent with the previous spectra of benzene on metal surfaces where benzene adsorbs with its molecular plane parallel to the surface. Namely, when the benzene molecule is π-bonded to a metal surface, its gas-phase symmetry of D_{6h} is reduced to at least C_{6v} and the only dipole-active modes would include C-H stretching modes, ring modes, and out-of-plane C-H bending modes.[79, 80] In contrast, the IRRAS spectrum of the FLN-55-coated Pt electrode shows only a trace of the most intense out-of-plane C-H bend at 670 cm^{-1}. Therefore, the IRRAS study confirms that the phenyl adsorption of the BPN-coated Pt is more significant than that of the FLN-55-coated Pt.

Microelectrode study on phenyl group adsorption

The impact of phenyl group adsorption on Pt-Ru/C catalyst is investigated using a microelectrode half-cell. The impact of phenyl group adsorption of the Pt-based catalyst is well documented in our previous publications.[61, 62] For this study, we measured the HOR voltammograms of Pt-Ru/C microelectrodes in contact with the BPN or FLN-55 thin film from 0.0 to 1.2 V vs. RHE. The HOR voltammogram of the Pt-Ru/C in contact with BPN is significantly suppressed between 0.02 and 0.7 V, indicating that phenyl group adsorption substantially inhibits the HOR activity of Pt-Ru/C (Fig. 6). In contrast, the Pt-Ru/C in contact with FLN-55 shows a typical HOR shape like the HOR voltammogram of catalyst in alkali-metal electrolytes:[61] the HOR current increases with the potential and reaches the limiting current density at 0.1 V vs. RHE. The HOR voltammogram shows that the intrinsic HOR activity of Pt-Ru in contact with BPN and FLN-55 is almost the same, *ca.* 0.1 mA cm^{-2} at 0.01 V vs. RHE, indicating that the phenyl group adsorption at the low potential is minimal. The low degree of phenyl group adsorption at the low potential range is probably due to the inhibition of the parallel phenyl group adsorption by the hydrogen evolution at the negative

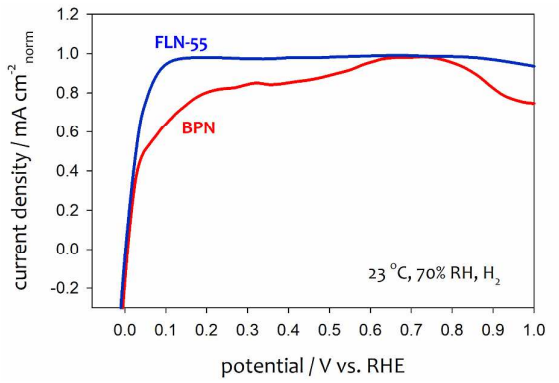

Figure 6. HOR voltammograms of Pt-Ru/C microelectrode in contact with BPN or FLN-55 thin-film. The voltammograms were measured in saturated H_2 environment at 23 °C, 70 % RH. Scan rate: 5 mV s^{-1}, normalized the current density by the limiting current density.

potential.[81] With further increase of the cell potential, however, the HOR current of Pt-Ru in contact with the BPN thin film is significantly suppressed until the cell potential reaches relatively high potential, *ca.* 0.7 V. Considering that the electrochemical properties of FLN-55 are similar to those of BPN, this result suggests that the difference in anode performance of MEAs employing the BPN and FLN ionomers may be caused by the phenyl group adsorption.

AMFC performance employing the BPN and FLN ionomers

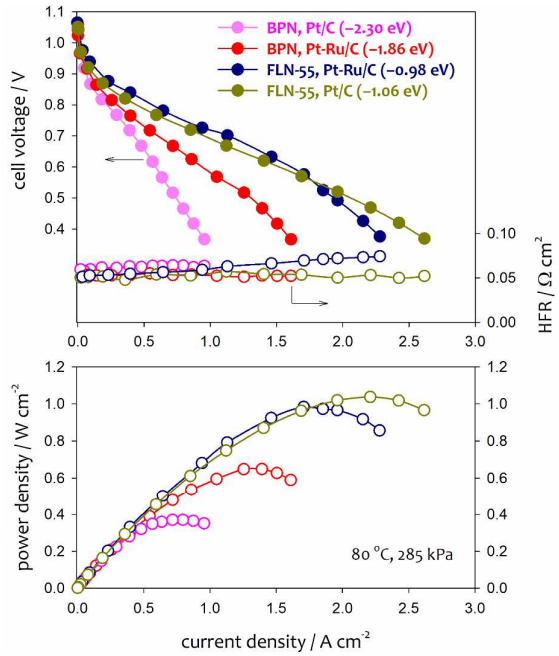

Figure 7. AMFC performance of MEAs employing the BPN and FLN-55 ionomers. Measured at 80 °C under H_2/O_2 with fully humidified H_2 (500 sccm) and O_2 (300 sccm) at 285 kPa backpressure after cell break-in at a constant voltage of 0.5 V for 24 h, Cathode: Pt/C (0.6 mg_{Pt} cm^{-2}), Anode: Pt/C (0.6 mg_{Pt} cm^{-2}) or Pt-Ru/C (0.5 mg_{Pt} cm^{-2}). Typically the peak power density of the AMFC increases ~ 40% after the break-in process (Fig. S7).

We evaluated the AMFC performance using different IEC of FLNs before investigating the structural effects of the ionomers. Figure S8 shows that the peak power density of the AMFC performance increased from 630 to 980 mW cm^{-2}, as the IEC of the FLN ionomers increased from 1.5 to 2.5 meq. g^{-1}. Note that the performance difference between the FLN ionomers is significant, considering that the hydroxide conductivity values of the FLN ionomers at 80 °C are similar (105–120 mS cm^{-1}). Further increase of the IEC of FLN to 3.5 meq. g^{-1} (FLN-100) resulted in lower performance due to the anode flooding.

The impact of the ionomer structure on AMFC performance is further studied with FLN-55 (IEC = 2.5 meq. g^{-1}) and BPN (IEC = 2.6 meq. g^{-1}) (Fig. 7). When the BPN ionomer was used with Pt/C catalyst in the electrodes, the peak power density was only 374 mW cm^{-2}. When the Pt/C anode catalyst was replaced with Pt-Ru/C catalyst, the peak power density of the AMFC significantly increased to 666 mW cm^{-2}, despite the similar cell high-frequency resistance (HFR), ~0.06 Ω cm^2. This result is expected as DFT results show that the adsorption energy of biphenyl on the surface of Pt is much higher than that on the surface of Pt-Ru (-2.30 eV for Pt vs. 1.86 eV for Pt-Ru). When the FLN-55 ionomer was used under the same conditions, the peak power density of the AMFC further increased to ~ 1000 mW cm^{-2} for both Pt/C and Pt-Ru/C anode-catalysed MEAs. The Pt-Ru/C anode catalysed MEA with FLN-55 exhibited slightly better performance at low current densities, *ca.* < 1.75 A cm^{-2}, than Pt/C anode catalysed MEA due to less phenyl group adsorption. However, the performance benefits from the less phenyl group adsorbed Pt-Ru/C catalyst diminished at the high current densities, probably due to the more hydrophobic nature of Pt/C catalyst, which may help reactant gas transport at the high current densities. The similar AMFC performance of the Pt/C and Pt-Ru/C anode catalysed MEAs employing FLN-55 suggests that the impact of phenyl group adsorptions for the FLN-55 bonded anodes between the Pt/C and Pt-Ru/C catalysts may be insignificant, which is consistent with our DFT calculation results that show the adsorption energy of 9,9-dimethyl fluorene on Pt and Pt-Ru is similar (-1.06 eV for Pt vs. -0.98 eV for Pt-Ru). The strong correlation between the AMFC performance and the adsorption energy of phenyl group of the ionomers on the HOR catalyst indicates that the phenyl group adsorption plays a critical role in AMFC performance.

On the other hand, water uptake of ionomer does not correlate well with the AMFC performance; the AMFC performance of the MEA with BPN was much inferior to that with FLN-40 even though the water uptake of BPN is about twice higher than that of FLN-40 (see Fig. S8 and Fig. 7 for AMFC performance comparison and Table 1 for water uptake). This result suggests that the performance improvement with the FLN ionomers is not due to better water management in MEA but due to the minimal ionomer-catalyst interaction at the anode.

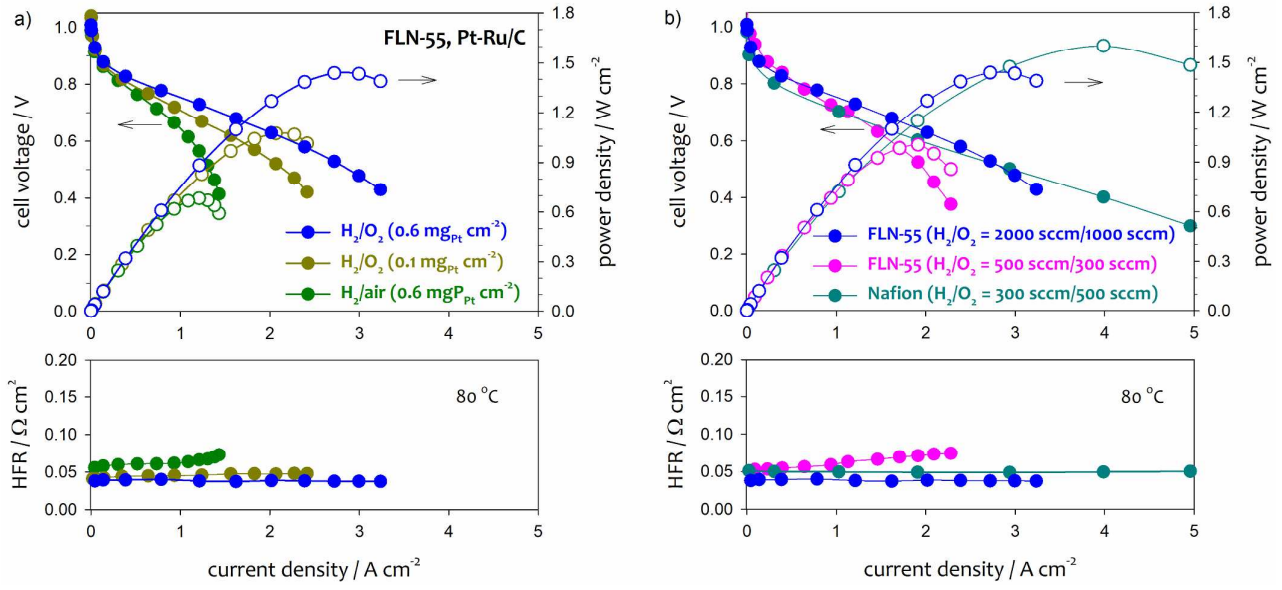

Figure 8. (a) Impact of operating conditions for AMFC performance of MEAs employing the FLN-55 ionomer. Measured the AMFC performance at 80 °C with fully humidified H_2 (2000 sccm) and O_2 (or air) (1000 sccm) at 285 kPa backpressure. Anode: Pt-Ru/C (0.5 or 0.1 mg_{Pt} cm^{-2}), cathode: Pt/C (0.6 mg_{Pt} cm^{-2}). (b) Performance comparison between AMFC and PEMFC. AMFC MEA: TPN membrane (thickness: 30 μm), FLN-bonded Pt-Ru alloy anode (0.5 mg_{Pt} cm^{-2}) and FLN-bonded Pt cathode (0.6 mg_{Pt} cm^{-2}). PEMFC MEA: Nafion membrane (thickness: 30 μm), Nafion-bonded Pt anode and cathode (0.6 mg_{Pt} cm^{-2}). All fuel cells were operated under same conditions except the anode and cathode flow rates. Operating temperature: 80 °C, backpressure: 285 kPa, 100% humidification.

The AMFC performance of MEA using the FLN-55 ionomer and Pt-Ru anode catalyst is further evaluated under different operating conditions. With increased anode flow rate to 2000 sccm, the H_2/O_2 AMFC performance further improved to generate the peak power density = 1,460 mW cm^{-2} (Fig. 8a). We observed similar anode flow rate effect for other MEAs; The MEA employing the BPN ionomer and Pt-Ru anode catalyst showed the peak power density of ~1200 mW cm^{-2} (Fig. S9) and the MEA with the FLN ionomer and Pt anode catalyst exhibited the peak power density of ~1300 mW cm^{-2} (Fig. S10). Requiring high H_2 flow rate for the better AMFC performance suggests that H_2 mass transport in the catalyst layer limits the performance of the AMFC. Under H_2/CO_2-free air conditions, the MEA showed lower AMFC performance with the peak power density = 682 mW cm^{-2}, as the O_2 partial vapour pressure decreases. The AMFC performance with lower Pt loading (0.1 mg_{Pt} cm^{-1}) of the Pt-Ru anode catalyst still exhibited over 1,000 mW cm^{-2} of peak power density.

We compare the cell performance between the FLN-55-based MEA and the Nafion-based PEMFC MEA operated at 80 °C (Fig. 8b). Note that good thermo-oxidative and alkaline-stability of the quaternized polyaromatic electrolytes used in this paper allows the AMFC operation at 80 °C. The cell HFR for all fuel cells are comparable, ~ 0.06 Ω cm^2, indicating that the cell resistance of the AMFC is close to that of the PEMFC with similar thickness of the Nafion membrane. The result shows that the FLN-55-based MEA outperformed the Nafion-based MEA at low current densities, *ca.* < 1 A cm^{-2}. This may be due to the lower gas crossover of the polyaromatic membrane *vs.* perfluorinated Nafion as well as a better oxygen reduction kinetics of Pt under high pH conditions. This result also suggests that the superior oxygen reduction reaction (ORR) activity can compensate the slow HOR activity of catalysts under high pH conditions. At high current densities, on the other hand, the Nafion-based MEA outperforms the FLN-55-based MEA. As a result, the peak power density of the AMFC is slightly less than that of the PEMFC. Considering that the HFR values of both MEAs are similar, this confirms that limited gas transport is a remaining issue for the polyaromatics-based MEA.

Finally, we examined the stability of the AMFC. Extended-term test of MEA using the FLN-55 ionomer was performed at a constant current (0.6 A cm^{-2}) to evaluate the durability of the AMFC and components' degradation. Fig. 9 shows the polarization curves and HFR during extended-term test. The AMFC performance was stable for the first 210 h and decreased slightly after 350 h, *ca.* 30 mV at 1.5 A cm^{-2} after 350 h. More notable performance loss occurred over the next 200 h fuel cell operation. In contrast to the performance degradation over time, the HFR of the cell remained stable during the extended-term test. This result indicates that the TPN AEM is stable during the continuous fuel cell operation. We believe that the degradation of electrocatalysts[82], as well as the disintegration of electrode three-phase interface[83], is responsible for the performance loss of the fuel cell devices. The durability of the AMFC is much inferior to that of Nafion-based PEMFCs which typically have a marginal loss after thousands of hours of operation under dynamic load conditions.

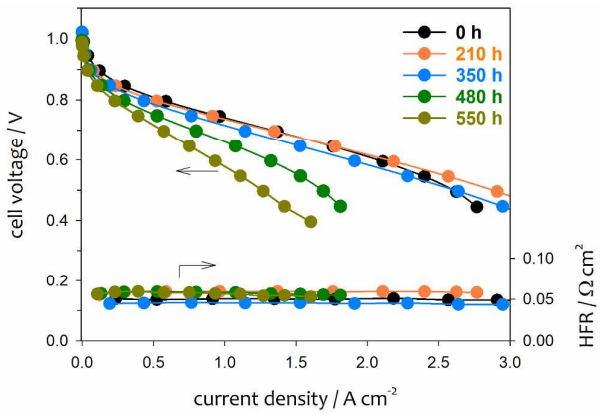

Figure 9. AMFC performance change of MEAs employing the FLN-55 ionomer during extended-term test. Measured the AMFC performance at 80 °C with fully humidified H_2 (2000 sccm) and O_2 (1000 sccm) at 285 kPa backpressure. Anode: Pt-Ru/C (0.5 mg_{Pt} cm^{-2}), cathode: Pt/C (0.6 mg_{Pt} cm^{-2}). The extended-term test was performed at a constant current density of 0.6 A cm^{-2} at 80 °C.

Conclusions

Utilizing high-performing aryl ether-free polyaromatic ionomers is beneficial for operating AMFCs at elevated temperatures with improved catalyst reaction kinetics. We have demonstrated that the AMFC performance using alkaline-stable aryl ether-free polyaromatics significantly improves due to quaternized poly(fluorene), which minimizes the phenyl group adsorption on HOR catalysts. Namely, the AMFC performance with alkylammonium functionalized poly(fluorene) ionomer approaches the PEMFC performance with Nafion-based MEA. After the excellent AMFC performance achieved by PoCelltech Inc.[1] and Mustain et al.[60] using PVBA-based ionomers, this is the first time a peak power density exceeding 1 W cm^{-2} using aryl ether-free polyaromatic ionomers is demonstrated. The positive impact of replacing the rotatable phenyl group in BPN with the non-rotatable phenyl group in FLN is greater than that of replacing Pt with the less phenyl group adsorbing Pt-Ru anode catalyst. Further performance improvement may be possible by developing less phenyl group adsorbing ionomers as the DFT calculation indicates that phenyl group adsorption on the surface of Pt-Ru catalyst is still favourable even with 9,9-dimethyl fluorene.

In our perspective, one remaining unresolved performance issue associated with aryl ether-free polyaromatics-based MEAs is the H_2 mass transport limitation, although it is unclear whether the mass transport issue is derived from the lack of hydrophobicity of the electrode[84] or the undesirable cation-hydroxide-water co-adsorption[85]. Anode flooding may also negatively impact the performance when more hydrophilic ionomers such as FLN-100 or more hydrophilic HOR catalysts such as Pd/C[86] are used. Long-term stability of AMFC system is

another remaining challenge even with MEAs employing alkaline-stable quaternized polyaromatics. Material interactions under the AMFC operating conditions need to be further understood. Development of PGM-free and low PGM catalysts for HOR and ORR without sacrificing AMFC performance may be the future direction to develop advanced AMFC technologies for economically competitive systems.

Conflicts of interest

There are no conflicts to declare.

Acknowledgements

The U.S. Department of Energy (US DOE), Office of Energy Efficiency and Renewable Energy (EERE), Fuel Cell Technologies Office (FCTO) supported this work under contract no. DE-AC52-06NA25396 (Los Alamos National Laboratory). We thankfully acknowledge the computational resources from the Tri-Lab computing resources of LANL, operated by Los Alamos National Security, LLC, for the National Nuclear Security Administration of U.S. Department of Energy (Contract DE-AC52-06NA25396), computational resources of NERSC, a DOE Office of Science User Facility supported by the Office of Science of the U.S. Department of Energy under Contract No. DE-AC02-05CH11231, and CNMS, which is a DOE Office of Science User Facility. VASP license was provided by Theoretical Division, LANL. CB thanks U.S. Department of Energy (ARPA-E, IONICS DE-FOA-0001478) for partial support of this project. This paper has been designated LA-UR-18-20472.

Notes and references

1. S. Gottesfeld, D. R. Dekel, M. Page, B. Bae, Y. S. Yan, P. Zelenay and Y. S. Kim, *J. Power Sources*, 2018, **375**, 170-184.
2. C. Arges and L. Zhang, *ACS Appl. Energy Mater.*, 2018, **1**, 2991-3012.
3. J. R. Varcoe, P. Atanassov, D. R. Dekel, A. M. Herring, M. A. Hickner, P. A. Kohl, A. R. Kucernak, W. E. Mustain, K. Nijmeijer, K. Scott, T. W. Xu and L. Zhuang, *Energy Environ. Sci.*, 2014, **7**, 3135-3191.
4. G. Merle, M. Wessling and K. Nijmeijer, *J. Membr. Sci.*, 2011, **377**, 1-35.
5. E. J. Park and Y. S. Kim, *J. Mater. Chem. A*, 2018, **6**, 15456-15477.
6. P. Zschocke and D. Quellmalz, *J. Membr. Sci.*, 1985, **22**, 325-332.
7. A. Warshawsky and O. Kedem, *J. Membr. Sci.*, 1990, **53**, 37-44.
8. K. C. Neyerlin, H. A. Gasteiger, C. K. Mittelsteadt, J. Jorne and W. B. Gu, *J. Electrochem. Soc.*, 2005, **152**, A1073-A1080.
9. J. Fang and P. K. Shen, *J. Membr. Sci.*, 2006, **285**, 317-322.
10. J. F. Zhou, M. Unlu, J. A. Vega and P. A. Kohl, *J. Power Sources*, 2009, **190**, 285-292.
11. J. H. Wang, S. H. Li and S. B. Zhang, *Macromolecules*, 2010, **43**, 3890-3896.
12. J. Pan, S. F. Lu, Y. Li, A. B. Huang, L. Zhuang and J. T. Lu, *Adv. Funct. Mater.*, 2010, **20**, 312-319.
13. X. M. Yan, G. H. He, S. Gu, X. M. Wu, L. G. Du and H. Y. Zhang, *J. Membr. Sci.*, 2011, **375**, 204-211.
14. H. Zarrin, J. Wu, M. Fowler and Z. W. Chen, *J. Membr. Sci.*, 2012, **394**, 193-201.
15. A. Jasti, S. Prakash and V. K. Shahi, *J. Membr. Sci.*, 2013, **428**, 470-479.
16. X. M. Yan, S. Gu, G. H. He, X. M. Wu and J. Benziger, *J. Power Sources*, 2014, **250**, 90-97.
17. A. N. Lai, L. S. Wang, C. X. Lin, Y. Z. Zhuo, Q. G. Zhang, A. M. Zhu and Q. L. Liu, *ACS. Appl. Mater. Inter.*, 2015, **7**, 8284-8292.
18. Z. H. Gu, A. T. Herrmann, C. E. Stivala and A. Zakarian, *Synlett*, 2010, 1717-1722.
19. C. Fujimoto, D. S. Kim, M. Hibbs, D. Wrobleski and Y. S. Kim, *J. Membr. Sci.*, 2012, **423**, 438-449.
20. G. W. Li, J. Pan, J. J. Han, C. Chen, J. T. Lu and L. Zhuang, *J. Mater. Chem. A*, 2013, **1**, 12497-12502.
21. S. Gu, R. Cai, T. Luo, K. Jensen, C. Contreras and Y. S. Yan, *ChemSuschem.*, 2010, **3**, 555-558.
22. Y. K. Choe, C. Fujimoto, K. S. Lee, L. T. Dalton, K. Ayers, N. J. Henson and Y. S. Kim, *Chem. Mater.*, 2014, **26**, 5675-5682.
23. A. D. Mohanty, S. E. Tignor, J. A. Krause, Y. K. Choe and C. Bae, *Macromolecules*, 2016, **49**, 3361-3372.
24. A. Amel, L. Zhu, M. Hickner and Y. Ein-Eli, *J. Electrochem. Soc.*, 2014, **161**, F615-F621.
25. C. G. Arges and V. Ramani, *Proc. Natl. Acad. Sci. USA*, 2013, **110**, 2490-2495.
26. C. G. Arges, L. H. Wang, J. Parrondo and V. Ramani, *J. Electrochem. Soc.*, 2013, **160**, F1258-F1274.
27. C. G. Arges, L. H. Wang, M. S. Jung and V. Ramani, *J. Electrochem. Soc.*, 2015, **162**, F686-F693.
28. L. Liu, S. Q. He, S. F. Zhang, M. Zhang, M. D. Guiver and N. W. Li, *ACS Appl. Mater. Inter.*, 2016, **8**, 4651-4660.
29. L. Zhu, J. Pan, C. M. Christensen, B. C. Lin and M. A. Hickner, *Macromolecules*, 2016, **49**, 3300-3309.
30. M. Irfan, E. Bakangura, N. U. Afsar, M. M. Hossain, J. Ran and T. W. Xu, *J. Power Sources*, 2017, **355**, 171-180.
31. L. Liu, X. Chu, J. Liao, Y. Huang, Y. Li, Z. Ge, M. A. Hickner and N. Li, *Energy Environ. Sci.*, 2018, **11**, 435-446.
32. W. H. Lee, Y. S. Kim and C. Bae, *ACS Macro. Lett.*, 2015, **4**, 814-818.
33. H. Ono, J. Miyake, S. Shimada, M. Uchida and K. Miyatake, *J. Mater. Chem. A*, 2015, **3**, 21779-21788.
34. W. H. Lee, E. J. Park, J. Han, D. W. Shin, Y. S. Kim and C. Bae, *ACS Macro. Lett.*, 2017, **6**, 566-570.
35. J. Pan, Y. Li, J. J. Han, G. W. Li, L. S. Tan, C. Chen, J. T. Lu and L. Zhuang, *Energy Environ. Sci.*, 2013, **6**, 2912-2915.
36. L. Zhu, J. Pan, Y. Wang, J. J. Han, L. Zhuang and M. A. Hickner, *Macromolecules*, 2016, **49**, 815-824.
37. J. J. Han, L. Zhu, J. Pan, T. J. Zimudzi, Y. Wang, Y. Q. Peng, M. A. Hickner and L. Zhuang, *Macromolecules*, 2017, **50**, 3323-3332.
38. D. Guo, C. X. Lin, E. N. Hu, L. Shi, F. Soyekwo, Q. G. Zhang, A. M. Zhu and Q. L. Liu, *J. Membr. Sci.*, 2017, **541**, 214-223.
39. L. Zhu, X. D. Yu and M. A. Hickner, *J Power Sources*, 2018, **375**, 433-441.
40. J. J. Han, Q. Liu, X. Q. Li, J. Pan, L. Wei, Y. Wu, H. Q. Peng, Y. Wang, G. W. Li, C. Chen, L. Xiao, J. T. Lu and L. Zhuang, *ACS Appl. Mater. Inter.*, 2015, **7**, 2809-2816.
41. Z. J. Yang, J. H. Zhou, S. W. Wang, J. Q. Hou, L. Wu and T. W. Xu, *J. Mater. Chem. A*, 2015, **3**, 15015-15019.
42. H. S. Dang and P. Jannasch, *J. Mater. Chem. A*, 2016, **4**, 11924-11938.

43. P. Jannasch and E. A. Weiber, *Macromol. Chem. Phys.*, 2016, **217**, 1108-1118.
44. X. Gong, X. M. Yan, T. T. Li, X. M. Wu, W. T. Chen, S. Q. Huang, Y. Wu, D. X. Zhen and G. H. He, *J. Membr. Sci.*, 2017, **523**, 216-224.
45. L. Zhu, T. J. Zimudzi, Y. Wang, X. D. Yu, J. Pan, J. J. Han, D. I. Kushner, L. Zhuang and M. A. Hickner, *Macromolecules*, 2017, **50**, 2329-2337.
46. C. Yang, L. Liu, X. J. Han, Z. G. Huang, J. P. Dong and N. W. Li, *J. Mater. Chem. A*, 2017, **5**, 10301-10310.
47. J. Pan, J. J. Han, L. Zhu and M. A. Hickner, *Chem. Mater.*, 2017, **29**, 5321-5330.
48. H. S. Dang and P. Jannasch, *Macromolecules*, 2015, **48**, 5742-5751.
49. H. S. Dang, E. A. Weiber and P. Jannasch, *J. Mater. Chem. A*, 2015, **3**, 5280-5284.
50. M. R. Hibbs, *J. Polym. Sci. Pol. Phys.*, 2013, **51**, 1736-1742.
51. R. Akiyama, N. Yokota, K. Otsuji, K. Miyatake, *Macromolecules*, 2018, **51**, 3394-3404.
52. Y. Wang, G. W. Wang, G. W. Li, B. Huang, J. Pan, Q. Liu, J. J. Han, L. Xiao, J. T. Lu and L. Zhuang, *Energy Environ. Sci.*, 2015, **8**, 177-181.
53. A. L. Ong, S. Saad, R. Lan, R. J. Goodfellow and S. W. Tao, *J. Power Sources*, 2011, **196**, 8272-8279.
54. R. Wycisk, D. Barpaga, S. Pintauro, M. D. Levan and P. N. Pintauro, *Adsorption*, 2014, **20**, 261-266.
55. C. G. Arges, L. H. Wang, J. Parrondo and V. Ramani, *Polymer Electrolyte Fuel Cells 13 (PEFC 13)*, 2013, **58**, 1551-1561.
56. A. M. A. Mahmoud, A. M. M. Elsaghier, K. Otsuji and K. Miyatake, *Macromolecules*, 2017, **50**, 4256-4266.
57. M. Mamlouk, J. A. Horsfall, C. Williams and K. Scott, *Int. J. Hydrog. Energy*, 2012, **37**, 11912-11920.
58. L. Wang, E. Magliocca, E. L. Cunningham, W. E. Mustain, S. D. Poynton, R. Escudero-Cid, M. M. Nasef, J. Ponce-Gonzalez, R. Bance-Soualhli, R. C. T. Slade, D. K. Whelligan and J. R. Varcoe, *Green Chem.*, 2017, **19**, 831-843.
59. L. Q. Wang, J. J. Brink, Y. Liu, A. M. Herring, J. Ponce-Gonzalez, D. K. Whelligan and J. R. Varcoe, *Energy Environ. Sci.*, 2017, **10**, 2154-2167.
60. T. J. Omasta, A. M. Park, J. M. Lamanna, Y. Zhang, X. Peng, L. Wang, D. L. Jacobson, J. R. Varcoe, D. S. Hussey, B. Pivovar and W. E. Mustain, *Energy Environ. Sci.*, 2018, **11**, 551-558.
61. I. Matanovic, H. T. Chung and Y. S. Kim, *J. Phys. Chem. Lett.*, 2017, **8**, 4918-4924.
62. S. Maurya, C. H. Fujimoto, M. R. Hibbs, C. N. Villarrubia and Y. S. Kim, *Chem. Mater.*, 2018, **30**, 2188-2192.
63. B. C. Lin, L. H. Qiu, B. Qiu, Y. Peng and F. Yan, *Macromolecules*, 2011, **44**, 9642-9649.
64. W. H. Lee, A. D. Mohanty and C. Bae, *ACS Macro. Lett.*, 2015, **4**, 453-457.
65. M. Tanaka, M. Koike, K. Miyatake and M. Watanabe, *Polym. Chem.*, 2011, **2**, 99-106.
66. W. H. Mei, C. L. Lu, J. L. Yan and Z. Wang, *RSC Adv.*, 2014, **4**, 47206-47206.
67. P. Y. Xu, K. Zhou, G. L. Han, Q. G. Zhang, A. M. Zhu and Q. L. Liu, *ACS Appl. Mater. Interfaces*, 2014, **6**, 6776-6785.
68. M. Dion, H. Rydberg, E. Schroder, D. C. Langreth and B. I. Lundqvist, *Phys. Rev. Lett.*, 2004, **92**.
69. G. Roman-Perez and J. M. Soler, *Phys. Rev. Lett.*, 2009, **103**.
70. J. Klimes, D. R. Bowler and A. Michaelides, *Phys. Rev. B*, 2011, **83**.
71. S. Babanova, I. Matanovic and P. Atanassov, *ChemElectrochem*, 2014, **1**, 2017-2028.
72. O. Bastiansen and S. Samdal, *J. Mol. Struct.*, 1985, **128**, 115-125.
73. M. P. Johansson and J. Olsen, *J. Chem. Theory Comput.*, 2008, **4**, 1460-1471.
74. A. B. Anderson, M. R. Devitt and F. L. Urbach, *Surf. Sci.,* 1984, **146**, 80.
75. E. L. Garfunkel and C. Minot, C.; Gavezzotti, A.; Simonetta, M. *Surf. Sci.*, 1986, **167**, 177.
76. Z. Jing and J. L. Whitten, *Surf. Sci.,* 1991, **250**, 147.
77. M. K. Sabbe, L. Lain, M. F. Reyniers and G. B. Marin, *Phys. Chem. Chem. Phys.*, 2013, **15**, 12197-12214.
78. S.-D. Yim, H. T. Chung, J. Chlistunoff, D.-S. Kim, C. Fujimoto, T.-H. Yang and Y. S. Kim, *J. Electrochem. Soc.*, 2015, **162**, F499-F506.
79. S. Haq and D. A. King, *J. Phys. Chem.*, 1996, **100**, 16957-16965.
80. N Sheppard, Ann. *Rev. Phys. Chem.*, 1988, **39**, 589-644.
81. H. T. Chung, Y. K. Choe, U. Martinez, J. H. Dumont, A. Mohanty, C. Bae, I. Matanovic and Y. S. Kim, *J. Electrochem. Soc.*, 2016, **163**, F1503-F1509.
82. A. Zadick, L. Dubau, N. Sergent, G. Berthome and M. Chatenet, *ACS Catal.*, 2015, **5**, 4819-4824.
83. D. A. Langlois, A. S. Lee, N. Macauley, S. Maurya, M. Hawley, S. D. Yim and Y. S. Kim, *J. Power Sources*, 2018, **396**, 345-354.
84. T. J. Omasta, L. Wang, X. Peng, C. A. Lewis, J. R. Varcoe and W. E. Mustain, *J. Power Sources*, 2018, **375**, 205-213.
85. H. T. Chung, U. Martinez, J. Chlistunoff, I. Matanovic and Y. S. Kim, *J. Phys. Chem. Lett.*, 2016, **7**, 4464-4469.
86. S. Maurya, J. Dumont, C. Narvaez Villarrubia, I. Matanovic, D. Li, Y. S. Kim, S. Noh, J. Han, C. Bae, H. A. Miller, C. H. Fujimoto, D. R. Dekel, *ACS. Catal.* 2018, DOI: 10.1021/acscatal.8b-3227.

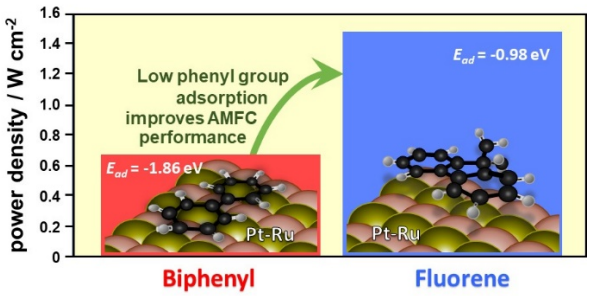

High-performance of polyaromatic alkaline membrane fuel cells was achieved with a polyfluorene ionomer with minimizing adsorption on hydrogen oxidation catalysts